

Fitting missing data by means of adaptive meshes of Bézier curves

M. A. Fortes^{*,a}, E. Medina^b

^a *Department of Applied Mathematics. Faculty of Science. University of Granada.
Campo del Príncipe, s/n. 18071 Granada. Spain.*

^b *Department of Mathematics. Faculty of Science. University of Cádiz.
Polígono Río de San Pedro, s/n. 11510 Puerto Real, Cádiz. Spain*

Abstract

In this paper we present a method to fit missing data -i.e., to fit a dataset containing a region in which no data are provided- by means of a C^1 -quadratic patch. Such a patch is constructed to faithfully extend the shape and the geometric features of the dataset. To this end, a mesh of curves gathering the information about the *shape* of the dataset will be considered and extended to the interior of the hole. Next, a (unique) patch fitting such a mesh of curves will be computed. Several numerical and graphical examples showing the effectiveness of the proposed method are provided.

Keywords: Powell-Sabin finite element; missing data; surface reconstruction; energy functional; shape-preserving; Bézier curves.

1. Introduction.

The problem of handling sets of scattered data points in which there is some hidden region, some lack of information -usually due to imperfections of the surface or solid to be scanned, to difficulties linked to the scan process, or to accessibility limitations, occlusions, reflecting spaces or surfaces parallel to camera- is rather common. This situation arises in all sorts of fields in which image reconstruction is involved: engineering problems, 3D human body scanning, dental reconstruction, archaeology, CAGD, Earth Sciences, computer vision in robotics, image reconstruction from satellite and radar information, physics, etc. Several papers in the literature address the question of fitting under these geometrical

*Corresponding author

Email address: mafortes@ugr.es; elena.medina@uca.es (M. A. Fortes^{*,a}, E. Medina^b)

difficulties or, more in general, under obstacles due to the dataset itself or to geometrical features or other additional constraints to be achieved.

Regarding the problem of fitting with additional drawbacks, we also find the one of fitting *missing data*, i.e., handling of datasets containing regions where no information -or information with not enough quality- is provided, or the more general of having a surface -understood as the graphic of a bivariate function- suffering from such a lack of information -a *hole*-. Most of the fitting missing data methods considered up to now are developed for arbitrary dataset points, i.e., they do not specifically consider the particular geometric feature of the dataset to be fitted. Applying these common fitting methods very often give rise to surfaces that tend to be ‘flat’ insofar as a reasonable way to define a patch is by minimizing some kind of measure, like the stretching or the bending energy. As a consequence, most of the existing methods work well for certain functions (as long as they are ‘flat’), but they do not lead to proper results in other cases. To illustrate this fact we can consider, for example, the case of filling a hole of information in the top of a semisphere: Depending on what the role of the fitting patch will be, we may want to fill the hole with a ‘minimal’ criteria -i.e., minimizing some linked measure-, or we may want to fill the hole by a bending patch with *semispherical* shape. It is desirable then to develop methods to fit missing or unstructured data, or to fill holes, providing fitting or filling patches restoring characteristics of the models ([1]), sharp features ([2]) or fulfilling some specific geometrical constraints of industrial or design type, in such a way that the fitting patch will be no longer flat but faithful to the shape of the known dataset. In short, we may be more interested in obtaining a global fitting function faithful to the dataset than in obtaining a minimal fitting patch.

With the aim of obtaining fitting patches somehow *inheriting* the shape of the known information, several approaches have been considered: e.g., in [3] the authors propose a method consisting of minimizing energy functionals to extend the shape of the dataset towards the interior of the hole by means of a patch fitting not only the data, but also some of its ‘estimated’ partial derivatives. Nevertheless, most approaches do not specifically adapt to the particular shape of the data to be fitted. In this work we propose a fitting method over missing data which, for each specific dataset, ‘calibrates’ its shape by means of several representative curves. These curves will be extended over the missing data preserving, as much as possible, the shape they have over the known data, becoming somehow the cornerstones of the global fitting surface. Such *wireframe* of curves will therefore play an essential role as long as, not only will identify the behavior -near the boundary of the missing data- of the surface to be fitted, but it will also determine the geometry of the fitting patch, that is required to preserve the shape of the known surface.

All over the fitting process, we will be interested in obtaining C^1 -splines with

the minimum possible degree in order to simplify computational aspects. That's why we choose the \mathcal{C}^1 -quadratic Powell-Sabin finite element and, insofar we want to work with this finite element, the first step we will have to carry out will be to fit the scattered data points by means of a \mathcal{C}^1 -quadratic fitting surface. Next, the fitting method we propose will consist mainly of three steps:

- i)* To define the wireframe of curves inside the known surface gathering the information about its shape;
- ii)* To extend such a wireframe of curves towards the interior of the hole;
- iii)* To construct a fitting patch over the *filled* wireframe of curves in *ii*).

The single-variate fitting process referred to in *ii)* will be carried out by means of Bézier curves, which give a more natural and wide frame to work with geometric features as tangent lines, osculating planes or curvature and torsion ([4] is a basic handbook for Bézier techniques). Regarding *iii)*, it is to mention that a surface fitting method based on one-dimensional fittings was for the first time considered in [5]. Nevertheless, the method therein proposed suffers from two drawbacks: on the one hand, it sits on a cartesian wireframe of curves, restricting then to 'measure' the shape of the surface along straight lines parallel to the axis and not allowing, thus, to consider other paths better gathering the shape of the surface. On the other hand, the fitting method in [5] considers just interpolation of function and derivatives values at boundary points of the curves to be fitted, both drawbacks leading to a more restrictive fitting frame as long as derivatives values on their own do not, in general, give a complete insight of the geometry of a surface.

The fitting method we propose in this work leads, especially in the case of more irregularly shaped functions, to more accurate fitting patches. This fact is a direct consequence of improving two of the main aspects of previous fitting methods:

- i)* The wireframe over which the fitting patch lies is obtained by means of Bézier techniques, which allows to more faithfully extend inside the hole the shape of the surface to be fitted;
- ii)* The fitting patch fits a wireframe which is general enough -no longer cartesian- to more faithfully gather the information of the surface to be fitted.

Moreover, this method constitutes, to our knowledge, the first one in which the fitting patches are obtained by means of Bézier curves, that more properly deal with geometric features.

The paper is organized as follows: in Section 2 we briefly present a review of some papers in the literature regarding the general problem of fitting data and

the more specific one of fitting data under additional drawbacks. In Section 3 we briefly recall the basic concepts on Powell-Sabin triangulations and Bézier curves that will be used throughout the work. In Section 4 we deal with the problem that we want to solve: we fix the notation to be used, we formulate the problem and we show the existence and uniqueness of the solution. Section 5 is devoted to present several graphical and numerical examples which show the effectiveness of the method proposed. We end up with a conclusions section.

2. A brief review of fitting data methods.

Among the techniques commonly applied to data fitting problems we find, for example, *B-splines*, *radial basis functions (RBF)*, *algebraic fitting* or *discrete energy minimization*.

RBF-fitting methods (see e.g. [6] or [7]) have the advantages that are mesh-free and that they become a powerful tool when handling multidimensional fitting data, while B-spline fitting methods become computationally harder when fine meshes are considered. On the contrary, using B-splines has the advantage that insofar as the basis functions have small local supports, they lead to sparse matrix that, moreover, are symmetric and definite positive under some conditions on the basis functions. Besides, B-splines are easier to implement than RBF since they are piecewise polynomial functions, usually with low degree.

Algebraic surface fitting, consisting in fitting a dataset by means of a polynomial implicit surface $f(x, y, z) = 0$ where the coefficients of f are usually chosen to minimize the mean square distance from the dataset to the implicit surface, is a natural approach to the fitting problem. Apart from the fact that manipulating polynomials is computationally more efficient than doing it with arbitrary analytic functions, algebraic surfaces provide enough generality to accurately model almost all complicated rigid objects. On the contrary, this kind of fitting often suffers from instability and numerical problems (see e.g. [8] or [9] and references therein).

Discrete energy minimization is an extended model in computer vision. One key advantage of this method is that it allows to handle a great variety of problems related to this researching field, like image denoising, segmentation, motion estimation object, recognition and image editing. Nevertheless, modern vision problems involve complex models and larger datasets that give rise to hard energy minimization problems (see e.g. [10] or [11] and references therein).

Among the existing techniques developed to handle fitting data with additional constraints we find the *biharmonic optimization*, used to overcome the problem of the flatness of the surfaces or regions that some methods based on minimization of stretching or bending energy provide (see e.g. [12]); *transfinite interpolation*, used e.g. in [13] to construct a Hermite interpolant matching

values and normal derivatives of a given function on the boundary of a simply connected planar domain; or other advanced techniques, like the one developed in [14], where algorithms to handle weakly defined control points by means of B-spline surfaces are provided.

Two interesting papers in the surface modeling field are [15] and [16]. In [15] a freeform modeling framework for unstructured triangle meshes based on constraint shape optimization is presented. As in this paper, in [15] the authors also consider the minimization of quadratic energy functionals that is carried out by means of the corresponding Euler-Lagrange equations, leading to surfaces with minimal area, minimal surface bending, or minimal variation of linearized curvature. On the other hand, in [16] the authors explore discretizations of Laplacian and Laplacian gradient energies PDE's on meshes by using mixed finite elements, and they demonstrate applications in several geometric modeling problems. Particularly, they present several examples of hole filling by means of surfaces fulfilling preset region or curve constraints with prescribed tangents or curvatures.

3. Preliminaries.

Let $D \subset \mathbb{R}^2$ be a polygonal domain (an open, non-empty connected set) in such a way that \overline{D} admits a Δ^1 -type triangulation (Figure 1 left), defined as the ones induced by integer translates of $x = 0, y = 0$ and $x + y = 0$ (see e.g. [17]).

Given a Δ^1 -triangulation \mathcal{T} of \overline{D} , we will consider the associated Powell-Sabin triangulation \mathcal{T}_6 of \mathcal{T} (see e.g. [18]), which is obtained by joining an appropriate interior point Ω_T of each $T \in \mathcal{T}$ to the vertices of T and to the interior points $\Omega_{T'}$ of the neighbouring triangles $T' \in \mathcal{T}$ of T . When T has a side lying on the boundary of D , the point Ω_T is joined to the mid-point of this side, to the vertices of T and to the interior points $\Omega_{T'}$ of the neighbouring triangles $T' \in \mathcal{T}$ of T . Hence, the six micro-triangles inside any $T \in \mathcal{T}$ have the point Ω_T as a common vertex. There are several ways to consider appropriate points Ω_T ([19]), nevertheless, a good choice ([20]) is considering Ω_T to be the incenter of T , for all $T \in \mathcal{T}$ (Figure 1).

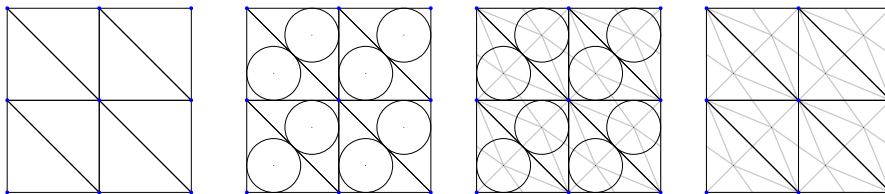


Figure 1: Δ^1 -type triangulation (left) and associated Powell-Sabin sub-triangulation (right).

Remark 1. It is well known ([19]) that given the values of a function f (defined on \bar{D}) and the ones of all its first partial derivatives at all the knots of \mathcal{T} , there exists a unique spline S in the space

$$\mathcal{S}_2^1(D, \mathcal{T}_6) = \{S \in C^1(D) : S|_{T'} \in \mathbb{P}_2(T') \quad \forall T' \in \mathcal{T}_6\},$$

where \mathbb{P}_2 stands for the space of bivariate polynomials of total degree at most two, such that the values of S and the ones of all its first partial derivatives coincide with those of f at all the knots of \mathcal{T} .

In what follows we will consider the usual inner semi-products $(u, v)_{m, X} := \sum_{|\omega|=m} \int_X \partial^\omega u(x) \partial^\omega v(x) dx$ and the semi-norms $|u|_{m, X} := (u, u)_{m, X}^{1/2}$, where $m = 0, 1, 2$; $X \subset D$ and u, v are any functions defined over X where the involved integrals can be considered. We will also consider the usual Euclidean norm $\langle \cdot, \cdot \rangle_n$ and Euclidean inner product $\langle \cdot, \cdot \rangle_n$ in \mathbb{R}^n .

Next we briefly recall some basic aspects of Bézier curves for the reader convenience. First, let us introduce the Bézier curve through the parametrization:

Definition 2. Given a set of $n + 1$ points $\{\mathbf{b}_0, \mathbf{b}_1, \dots, \mathbf{b}_n\}$, the n -degree polynomial curve parametrized by

$$\mathbf{b}(\tau) = \sum_{j=1}^n B_j^n(\tau) \mathbf{b}_j, \quad \tau \in [0, 1], \quad (1)$$

is referred to as the Bézier curve with control points $\{\mathbf{b}_0, \mathbf{b}_1, \dots, \mathbf{b}_n\}$. In (1) $B_j^n(s)$, $j = 0, \dots, n$ stand for the Bernstein polynomials defined by

$$B_j^n(\tau) := \binom{n}{j} \tau^j (1 - \tau)^{n-j} \quad \text{for } j = 0, \dots, n,$$

and $B_j^n \equiv 0$ if $j \in \mathbb{Z} \setminus \{0, 1, \dots, n\}$.

It can be easily checked that the Bernstein polynomials satisfies $\sum_{j=1}^n B_j^n(\tau) = 1$, so that for each $\tau \in [0, 1]$ equation (1) gives $\mathbf{b}(\tau)$ as an affine combination of the control points. The next proposition summarize the properties of the Bézier curve which will be used later.

Proposition 3. The Bézier curve satisfies the interpolation properties:

- The tangent line of the Bézier curve (1) at the end point $\mathbf{b}(0) = \mathbf{b}_0$ (resp. $\mathbf{b}(1) = \mathbf{b}_n$) is given by $\mathbf{b}_0 + \overrightarrow{\langle \mathbf{b}_0 \mathbf{b}_1 \rangle}$ (resp. $\mathbf{b}_n + \overrightarrow{\langle \mathbf{b}_n \mathbf{b}_{n-1} \rangle}$).
- The osculating plane of the curve (1) at the end point $\mathbf{b}(0) = \mathbf{b}_0$ (resp. $\mathbf{b}(1) = \mathbf{b}_n$) is given by $\mathbf{b}_0 + \overrightarrow{\langle \mathbf{b}_0 \mathbf{b}_1, \mathbf{b}_1 \mathbf{b}_2 \rangle}$ (resp. $\mathbf{b}_n + \overrightarrow{\langle \mathbf{b}_n \mathbf{b}_{n-1}, \mathbf{b}_{n-1} \mathbf{b}_{n-2} \rangle}$).

PROOF. Taking derivatives in (1) it is immediately found that

$$\begin{aligned}\dot{\mathbf{b}}(\tau) &= \frac{d\mathbf{b}}{d\tau}(\tau) = \sum_{j=0}^{n-1} B_j^{n-1}(\tau) \overrightarrow{\mathbf{b}_j \mathbf{b}_{j+1}}, \\ \ddot{\mathbf{b}}(\tau) &= \frac{d^2\mathbf{b}}{d\tau^2}(\tau) = \sum_{j=0}^{n-2} B_j^{n-2}(\tau) \left(\overrightarrow{\mathbf{b}_{j+1} \mathbf{b}_{j+2}} - \overrightarrow{\mathbf{b}_j \mathbf{b}_{j+1}} \right),\end{aligned}\tag{2}$$

thus, the tangent vector to the Bézier curve (1) at \mathbf{b}_0 is proportional to $\dot{\mathbf{b}}(0) = n \overrightarrow{\mathbf{b}_0 \mathbf{b}_1}$, whereas the direction of the osculating plane is generated by the vectors $\dot{\mathbf{b}}(0) = n \overrightarrow{\mathbf{b}_0 \mathbf{b}_1}$ and $\ddot{\mathbf{b}}(0) = n(n-1) \left(\overrightarrow{\mathbf{b}_1 \mathbf{b}_2} - \overrightarrow{\mathbf{b}_0 \mathbf{b}_1} \right)$, and consequently is given by $\langle \overrightarrow{\mathbf{b}_0 \mathbf{b}_1}, \overrightarrow{\mathbf{b}_1 \mathbf{b}_2} \rangle$. The tangent vector and the direction of the osculating plane at $\mathbf{b}(1) = \mathbf{b}_n$ are determined by substituting $\tau = 1$ in (2).

4. Formulation of the problem and main results.

As explained in the introduction, the objective of this work is to develop a method to fit missing data in a given dataset by means of a wireframe of ‘adaptive’ filled curves. To this aim, we will first introduce the notation to be used:

- ▷ *Hole*: Let H be a connected and nonempty subset of D (in Figures 2 and 15 left, we show the holes to be used in the examples provided in this work) such that $\partial D \cap \partial H = \emptyset$, where ∂X stands for the boundary of the set X . If H were not connected, the techniques developed in this work to fill one connected hole would be applied to each of the connected components of H . Let now $f : \overline{D} - H \rightarrow \mathbb{R}$ be a function. In order to reconstruct the missing data in the graphic of f over H , and taking into account that we are interested in working with spline functions defined over triangulations, we will extend the hole H to a polygonal one.
- ▷ *Triangulations*: Let \mathcal{T} be a Δ^1 -type triangulation of \overline{D} with associated Powell-Sabin triangulation \mathcal{T}_6 . Let

$$H^* = \bigcup_{\{T \in \mathcal{T} : T \cap H \neq \emptyset\}} T.$$

Thus, H^* is a polygonal domain surrounding H (Figure 2 right). Clearly, H^* tends to H as $\text{diam}(\mathcal{T}) \rightarrow 0$ (recall that the *diameter* of a triangulation \mathcal{T} is defined as $\text{diam}(\mathcal{T}) = \max_{x,y \in T} \|x - y\|$ for any $T \in \mathcal{T}$). We need to consider \mathcal{T} fine enough to have $\partial D \cap \partial H^* = \emptyset$. Let

$$\{t_1, \dots, t_s\}\tag{3}$$

be the set of all the vertices of \mathcal{T} laying on the boundary of H^* (Figure 2 right). Let

$$\mathcal{T}_{D-H^*} = \{T \in \mathcal{T} : T \subset D - H^*\} \text{ and } (\mathcal{T}_{D-H^*})_6 = \{T \in \mathcal{T}_6 : T \subset D - H^*\}.$$

It is clear then that \mathcal{T}_{D-H^*} is a Δ^1 -type triangulation of $\overline{D} - \overset{\circ}{H^*}$ with associated Powell-Sabin subtriangulation $(\mathcal{T}_{D-H^*})_6$. Analogously, let

$$\mathcal{T}_{H^*} = \{T \in \mathcal{T} : T \subset H^*\} \text{ and } (\mathcal{T}_{H^*})_6 = \{T \in \mathcal{T}_6 : T \subset H^*\},$$

in such a way that \mathcal{T}_{H^*} is a Δ^1 -type triangulation of H^* with associated Powell-Sabin subtriangulation $(\mathcal{T}_{H^*})_6$.

▷ *Functional spaces:* Let us consider the splines spaces

$$\mathcal{S}_2^1(D - H^*, (\mathcal{T}_{D-H^*})_6) = \{v|_{D-H^*} : v \in \mathcal{S}_2^1(D, \mathcal{T}_6)\} \quad \text{and}$$

$$\mathcal{S}_2^1(H^*, (\mathcal{T}_{H^*})_6) = \{v|_{H^*} : v \in \mathcal{S}_2^1(D, \mathcal{T}_6)\}.$$

In what follows, for the sake of simplicity, we will just denote $\mathcal{S}_2^1(D - H^*) \equiv \mathcal{S}_2^1(D - H^*, (\mathcal{T}_{D-H^*})_6)$ and $\mathcal{S}_2^1(H^*) \equiv \mathcal{S}_2^1(H^*, (\mathcal{T}_{H^*})_6)$ in the understanding that original triangulation \mathcal{T} is fixed but arbitrary.

The problem of filling the graphic of f over H^* is posed as follows:

Problem 4. *To define a global reconstructed function $\tilde{f} \in \mathcal{C}^1(D)$,*

$$\begin{aligned} \tilde{f} : D &\longrightarrow \mathbb{R} \\ \mathbf{x} &\longmapsto \begin{cases} s_f & \text{if } \mathbf{x} \in D - H^* \\ \sigma_{s_f} & \text{if } \mathbf{x} \in H^* \end{cases} \end{aligned}$$

in such a way that:

i) $\tilde{f} = s_f$ be as close as possible to f in $D - H^*$;

ii) $\tilde{f} = \sigma_{s_f}$ fills the hole of f over H^* .

Spline s_f over $D - H^*$ is defined as the minimal energy fitting surface provided in [21]. More precisely, s_f is the only one spline in $\mathcal{S}_2^1(D - H^*)$ minimizing the functional $\mathcal{J}_1 : \mathcal{S}_2^1(D - H^*) \longrightarrow \mathbb{R}$ defined by

$$\mathcal{J}_1(v) = \langle \rho(v - f) \rangle_q^2 + \lambda_1 |v|_{1,D-H^*}^2 + \lambda_2 |v|_{2,D-H^*}^2,$$

where $\lambda_1 \geq 0, \lambda_2 > 0$, ρ is the evaluation operator $\rho(v) = (v(p_1), \dots, v(p_q))$ and $\mathcal{P} = \{p_i\}_{i=1}^q$ is a subset of points in $D - H^*$. In [21] it is shown that s_f can be

expressed as $s_f = \sum_{i=1}^{\ell} \nu_i \gamma_i$, where $\{\gamma_1, \dots, \gamma_{\ell}\}$ is a basis of $\mathcal{S}_2^1(D - H^*)$ and $\boldsymbol{\nu} \equiv (\nu_i)_{i=1}^{\ell}$ is the solution to the linear system $A\mathbf{X} = b$, where

$$A = \left(\langle \rho(\gamma_i), \rho(\gamma_j) \rangle_q + \sum_{m=1}^2 \lambda_m (\gamma_i, \gamma_j)_{m, D-H^*} \right)_{i,j=1}^{\ell}$$

and $b = (\langle \rho(f), \rho(\gamma_i) \rangle_q)_{i=1}^{\ell}$.

We focus now on the construction of σ_{s_f} . Such a function will be constructed over a mesh of curves that, somehow, ‘inherits’ the geometry that dataset \mathcal{P} has outside the hole H^* . More precisely, let

$$\mathcal{Q} = \{\{Q_i^s, Q_i^e\}\}_{i=1}^p \quad (4)$$

be a set of couples of different points belonging all of them to ∂H^* in such a way that $\{(Q_i^s, s_f(Q_i^s)), (Q_i^e, s_f(Q_i^e))\}_{i=1}^p$ is a set of points lying on the inner boundary of the graphic of s_f . Let

$$\mathcal{P} = \{\{\xi_i^s, \xi_i^e\}\}_{i=1}^p, \quad (5)$$

with

$$\xi_i^s : (-\varepsilon_i^s, 0] \longrightarrow \mathbb{R}^2 \quad \text{and} \quad \xi_i^e : [0, \varepsilon_i^e] \longrightarrow \mathbb{R}^2, \quad (6)$$

be a set of couples of parametric curves, with $\varepsilon_i^s, \varepsilon_i^e > 0$, such that $\xi_i^s(0) = Q_i^s$; $\xi_i^e(0) = Q_i^e$ and their image sets $\xi_i^s((-\varepsilon_i^s, 0])$ and $\xi_i^e([0, \varepsilon_i^e])$ are contained in $D - H^*$. Then $(\xi_i^s, s_f \circ \xi_i^s)$ and $(\xi_i^e, s_f \circ \xi_i^e)$ is a set of parametric curves lying on the graphic of s_f with ending and starting points $(Q_i^s, s_f(Q_i^s))$ and $(Q_i^e, s_f(Q_i^e))$, respectively, for $i = 1, \dots, p$. In what follows, for the sake of simplicity, we will denote the compositions $s_f \circ \xi_i^s$ and $s_f \circ \xi_i^e$ just bust juxtaposition $s_f \xi_i^s$ and $s_f \xi_i^e$.

Let us consider the set

$$\mathcal{B} = \{\beta_i\}_{i=1}^p, \quad (7)$$

where, for $i = 1, \dots, p$, $\beta_i \equiv (\beta_{ix}, \beta_{iy}, \beta_{iz}) : [a_i, b_i] \rightarrow \mathbb{R}^3$ is a function verifying that the graphic of (β_{ix}, β_{iy}) , i.e., the projection of the graphic of β_i onto the XY plane, is contained in H^* ; and that $\beta_i(a_i) = (Q_i^s, s_f(Q_i^s))$ and $\beta_i(b_i) = (Q_i^e, s_f(Q_i^e))$, i.e., β_i is a parametric curve *filling* the graphics of the curves $(\xi_i^s, s_f \xi_i^s)$ and $(\xi_i^e, s_f \xi_i^e)$.

In the theoretical development that follows, any curves β_i verifying previous conditions can be considered, nevertheless, in the numerical section we will handle just with Bézier curves based on a more complete interpolation scheme as long as we will look for σ_{s_f} to preserve the shape of f as much as possible.

The filling function σ_{s_f} over H^* will be defined as the unique function in $\mathcal{S}_2^1(H_{s_f}^*) \equiv \{v \in \mathcal{S}_2^1(H^*) : \varphi(v) = \varphi(s_f)\}$, where $\varphi(v) = (\varphi_i(v))_{i=1}^{3s}$, with

$$\varphi_i(v) = v(t_i), \quad \varphi_{s+i}(v) = \frac{\partial v}{\partial x}(t_i), \quad \varphi_{2s+i}(v) = \frac{\partial v}{\partial y}(t_i), \quad \text{for } i = 1, \dots, s,$$

t_i being the knots in (3), minimizing the functional $\mathcal{J}_2 : \mathcal{S}_2^1(H_{s_f}^*) \rightarrow \mathbb{R}$ defined by

$$\mathcal{J}_2(v) = \sum_{i=1}^p \int_{a_i}^{b_i} (v \circ (\beta_{ix}, \beta_{iy}) - \beta_{iz})^2 + \tau_1 |v|_{1, H^*}^2 + \tau_2 |v|_{2, H^*}^2 \quad (8)$$

where $\tau_1 \geq 0, \tau_2 > 0$.

Observe that choosing $\sigma_{s_f} \in \mathcal{S}_2^1(H_{s_f}^*)$ is equivalent to impose σ_{s_f} to join to s_f with class \mathcal{C}^1 . In the next result we show the existence and uniqueness of σ_{s_f} .

Theorem 5. *There exists a unique $\sigma_{s_f} \in \mathcal{S}_2^1(H_{s_f}^*)$ minimizing functional \mathcal{J}_2 which is also the solution to the following variational problem:*

$$\left\{ \begin{array}{l} \text{Find } \sigma_{s_f} \in \mathcal{S}_2^1(H_{s_f}^*) \text{ such that} \\ \sum_{i=1}^p \int_{(\beta_{ix}, \beta_{iy})} \sigma_{s_f} \cdot v + \sum_{m=1}^2 \tau_m (\sigma_{s_f}, v)_{m, H^*} = \sum_{i=1}^p \int_{a_i}^{b_i} (v \circ (\beta_{ix}, \beta_{iy})) \cdot \beta_{iz} \\ \text{for all } v \in \mathcal{S}_2^1(H_{\mathbf{0}}^*) \equiv \{v \in \mathcal{S}_2^1(H^*) : \varphi(v) = \mathbf{0}\}. \end{array} \right. \quad (9)$$

PROOF. The proof follows the same pattern than the one of Theorem 4 in [5] when taking

$$a(u, v) = 2 \left(\sum_{i=1}^3 u(k_i)v(k_i) + \sum_{i=1}^p \int_{(\beta_{ix}, \beta_{iy})} u \cdot v + \sum_{m=1}^2 \tau_m (u, v)_{m, H^*} \right) \quad \text{and}$$

$$\psi(v) = 2 \sum_{i=1}^p \int_{a_i}^{b_i} (v \circ (\beta_{ix}, \beta_{iy})) \cdot \beta_{iz}.$$

Remark 6. *In order to compute σ_{s_f} verifying (9), let us consider the usual Hermite basis $\{w_i\}_{i=1}^{3s}$ associated to the knots $\{t_i\}_{i=1}^s$ of \mathcal{T} laying on the boundary of H^* , that is, the ones verifying $\varphi(w_i) = (0, \dots, 0, \overset{i}{1}, 0, \dots, 0)$ for all $i \in \{1, \dots, 3s\}$, and let us extend it to the usual Hermite basis $\{w_1, \dots, w_{3s}, w_{3s+1}, \dots, w_n\}$ of $\mathcal{S}_2^1(H^*)$, in such a way that $\{w_{3s+1}, \dots, w_n\}$ is a basis of $\mathcal{S}_2^1(H_{\mathbf{0}}^*)$. Then, the fact that $\sigma_{s_f} \in \mathcal{S}_2^1(H_{s_f}^*)$ together with equations (9) lead to the expression*

$$\sigma_{s_f} = \sum_{i=1}^{3s} \varphi_i(s_f) w_i + \sum_{j=3s+1}^n \alpha_{j-3s} w_j,$$

where the vector $(\alpha_j)_{j=1}^{n-3s}$ is the solution to the linear equations system $A\mathbf{X} = \mathbf{b}$, where:

$$A = \left(\sum_{j=1}^p \int_{(\beta_{ix}, \beta_{iy})} w_j \cdot w_t + \tau_1(w_j, w_t)_{1, H^*} + \tau_2(w_j, w_t)_{2, H^*} \right)_{j, t=3s+1}^n \quad \text{and}$$

$$b = \left(\sum_{i=1}^p \int_{a_i}^{b_i} \beta_{iz} \cdot w_t - \sum_{k=1}^{3s} \varphi_k(s_f) \left(\tau_1(w_k, w_t)_{1, H^*} + \tau_2(w_k, w_t)_{2, H^*} + \sum_{i=1}^p \int_{(\beta_{ix}, \beta_{iy})} w_k \cdot w_t \right) \right)_{t=3s+1}^n .$$

5. Graphical and numerical examples.

In this section, with the aim to show the effectiveness of the hole-filling method proposed, we present some examples obtained by means of several test functions and by using wireframes obtained according to different criteria.

In all cases we consider the domain $D = (0, 1) \times (0, 1)$; the Δ^1 -type triangulation \mathcal{T}^{10} associated to the uniform partition of each of the sides of D into 10 subintervals; a dataset \mathcal{P} consisting of $q = 5000$ points and the smoothing parameters $\lambda_1 = 10^{-3}$ and $\lambda_2 = 10^{-6}$ in functional \mathcal{J}_1 -such values have been tested to give proper fitting surfaces (see [22])-. In order to give the same weight to semi norms $|\cdot|_1$ and $|\cdot|_2$ inside and outside the hole, we have chosen $\tau_1 = 10^{-3}$ and $\tau_2 = 10^{-6}$ in functional \mathcal{J}_2 (8).

We have considered different test functions f_i , for $i = 1, \dots, 4$. Functions f_1, f_2 and f_3 have been carried out over the hole H_1 defined implicitly by

$$\frac{(x - 0.5)^2}{0.25^2} + \frac{(y - 0.5)^2}{0.125^2} \leq 1. \quad (10)$$

In Figure 2 we show the graphics of H_1, \mathcal{T}^{10} , the surrounding H_1^* and the set of boundary knots $\{t_i\}_{i=1}^s$ in (3).

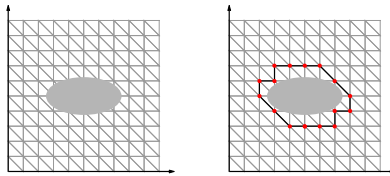


Figure 2: Triangulation \mathcal{T}^{10} , hole H_1 , polygonal hole H_1^* and set of knots $\{t_i\}_{i=1}^s$.

In all cases, to construct the wireframe of curves β (7) we have to choose the set of points (4), the curves (5) and the interpolation scheme to define the filling curves β_i . We have considered three different criteria, all of them based on Bézier techniques: *lines wireframe*, *contour lines wireframe* and *gradient lines wireframe*.

- *Lines wireframe*: The points Q_i^s and Q_i^e are chosen to be symmetric with respect to the centroid \mathcal{C} of the hole H^* . The functions ξ_i^s and ξ_i^e (6) are defined by

$$\begin{aligned}\xi_i^s(t) &= Q_i^s + t \overrightarrow{Q_i^s \mathcal{C}}, & t \in (-\varepsilon_i^s, 0], \\ \xi_i^e(t) &= Q_i^e + t \overrightarrow{\mathcal{C} Q_i^e}, & t \in [0, \varepsilon_i^e),\end{aligned}$$

with $\varepsilon_i^s, \varepsilon_i^e > 0$. In Figure 3 we show a couple of points (4) and curves (5) for the polygonal hole H_1^* considered in Figure 2.

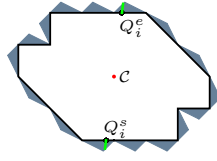


Figure 3: Points (Q_i^s, Q_i^e) and curves (ξ_i^s, ξ_i^e) for *lines wireframe*.

The filling function β_i is then defined as follows: for each $i = 1, \dots, p$, let $\mathbf{t}_i^s, \mathbf{t}_i^e$ and $\mathbf{n}_i^s, \mathbf{n}_i^e$ be the tangent and normal vectors to $(\xi_i^s, s_f \xi_i^s)$ and $(\xi_i^e, s_f \xi_i^e)$ at $(Q_i^s, s_f(Q_i^s))$ and $(Q_i^e, s_f(Q_i^e))$, respectively. In order to match the curves $(\xi_i^s, s_f \xi_i^s)$ and $(\xi_i^e, s_f \xi_i^e)$ we construct a fifth order Bézier curve with control points $\mathbf{b}_k, k = 0, \dots, 5$, such that

$$\begin{aligned}\mathbf{b}_0 &= (Q_i^s, s_f(Q_i^s)); & \mathbf{b}_1 &= (Q_i^s, s_f(Q_i^s)) + \sigma_1 \mathbf{t}_i^s; & \mathbf{b}_2 &= (Q_i^s, s_f(Q_i^s)) + \sigma_2 \mathbf{t}_i^s + \sigma_3 \mathbf{n}_i^s, \\ \mathbf{b}_5 &= (Q_i^e, s_f(Q_i^e)); & \mathbf{b}_4 &= (Q_i^e, s_f(Q_i^e)) - \sigma_6 \mathbf{t}_i^e; & \mathbf{b}_3 &= (Q_i^e, s_f(Q_i^e)) + \sigma_4 \mathbf{t}_i^e + \sigma_5 \mathbf{n}_i^e,\end{aligned}\quad (11)$$

with σ_l , for $l = 1, \dots, 6$, being unknown parameters (σ_1 and σ_6 positive). With the election of the control points given in (11) we ensure that

$$\begin{aligned}\langle \overrightarrow{\mathbf{b}_0 \mathbf{b}_1} \rangle &= \langle \mathbf{t}_i^s \rangle & \langle \overrightarrow{\mathbf{b}_0 \mathbf{b}_1}, \overrightarrow{\mathbf{b}_1 \mathbf{b}_2} \rangle &= \langle \mathbf{t}_i^s, \mathbf{n}_i^s \rangle, \\ \langle \overrightarrow{\mathbf{b}_4 \mathbf{b}_5} \rangle &= \langle \mathbf{t}_i^e \rangle & \langle \overrightarrow{\mathbf{b}_4 \mathbf{b}_5}, \overrightarrow{\mathbf{b}_3 \mathbf{b}_4} \rangle &= \langle \mathbf{t}_i^e, \mathbf{n}_i^e \rangle,\end{aligned}$$

so according to Proposition 3, both the tangent line and the osculating plane, are continuous at $(Q_i^s, s_f(Q_i^s))$ and $(Q_i^e, s_f(Q_i^e))$ when filling $(\xi_i^s, s_f \xi_i^s)$ and $(\xi_i^e, s_f \xi_i^e)$ with β_i . Next, we impose the curvature and the torsion to be also continuous at $(Q_i^s, s_f(Q_i^s))$ and $(Q_i^e, s_f(Q_i^e))$. These conditions determine the parameters $\sigma_1, \sigma_2, \sigma_4$ and σ_6 as functions of σ_3 and σ_5 (unless $(\xi_i^s, s_f \xi_i^s)$ and $(\xi_i^e, s_f \xi_i^e)$ lie in a common plane; in this case, the torsion continuity conditions are trivial and the curvature continuity conditions will provide us σ_1 and σ_6 in terms of $\sigma_2, \sigma_3, \sigma_4$ and σ_5). The parameters which have not been determined from the curvature and torsion continuity conditions are chosen to minimize the function

$$\sum_{k=0}^4 \|\overrightarrow{\mathbf{b}_k \mathbf{b}_{k+1}}\|^2, \quad (12)$$

as long as the vectors $\overrightarrow{\mathbf{b}_0\mathbf{b}_1}$ and $\overrightarrow{\mathbf{b}_4\mathbf{b}_5}$ (or equivalently σ_1 and σ_6) determined by using (12) are large enough. More precisely, we accept the result obtained by minimizing (12) provided that $\|\overrightarrow{\mathbf{b}_0\mathbf{b}_1}\|, \|\overrightarrow{\mathbf{b}_4\mathbf{b}_5}\| > 0.01$ is satisfied. Otherwise, the remaining unknown parameters are chosen such that they minimize $\frac{\sum_{k=0}^4 \|\overrightarrow{\mathbf{b}_k\mathbf{b}_{k+1}}\|^2}{\|\mathbf{b}_0\mathbf{b}_1\| \|\mathbf{b}_4\mathbf{b}_5\|}$.

Note that it is not possible to ensure continuity of tangent line, osculating plane, curvature and torsion in both end points $(Q_i^s, s_f(Q_i^s))$ and $(Q_i^e, s_f(Q_i^e))$ if a lower order Bézier curve is used. Indeed, we can get continuous tangent lines and osculating planes by using a fourth order Bézier curve with control points

$$\begin{aligned}\hat{\mathbf{b}}_0 &= (Q_i^s, s_f(Q_i^s)), & \hat{\mathbf{b}}_4 &= (Q_i^e, s_f(Q_i^e)), \\ \hat{\mathbf{b}}_1 &\in (Q_i^s, s_f(Q_i^s)) + \langle \mathbf{t}_i^s \rangle, & \hat{\mathbf{b}}_3 &\in (Q_i^e, s_f(Q_i^e)) + \langle \mathbf{t}_i^e \rangle, \\ \hat{\mathbf{b}}_2 &\in [(Q_i^s, s_f(Q_i^s)) + \langle \mathbf{t}_i^s, \mathbf{n}_i^s \rangle] \cap [(Q_i^e, s_f(Q_i^e)) + \langle \mathbf{t}_i^e, \mathbf{n}_i^e \rangle].\end{aligned}$$

However, in this case we only count on three free parameters (each of the control points $\hat{\mathbf{b}}_j, j = 1, 2, 3$ moves on a straight line), which in general cannot be chosen in order to satisfy the four remaining continuity conditions, i.e. continuity of curvature and torsion at both ends.

• *Contour lines wireframe:* For each $i = 1, \dots, p$, the starting point Q_i^s can be arbitrarily chosen over ∂H^* . Let T_i^s be the triangle of the Powell-Sabin subtriangulation $(\mathcal{T}_{D-H^*}^{10})_6$ containing the point Q_i^s . Since $s_f|_{T_i^s} \in \mathbb{P}_2(T_i^s)$, we have that the equation $s_f|_{T_i^s} = s_f(Q_i^s)$ is a conic, and thus it can be easily parametrized by means of a function ξ_i^s (such a parametrization can be chosen in such a way that $\xi_i^s(0) = Q_i^s$). Next, according to the contour lines map of s_f , we will be able of finding another point $Q_i^e \in \partial H^*$ belonging to the same contour line of s_f than Q_i^s . A process similar than the one developed for Q_i^s will provide us ξ_i^e verifying $\xi_i^e(0) = Q_i^e$. Now, filling the curves $(\xi_i^s(t), s_f(Q_i^s))$ and $(\xi_i^e(t), s_f(Q_i^e))$ consists just in obtaining (β_{ix}, β_{iy}) filling ξ_i^s and ξ_i^e , since β_{iz} can be prescribed as $s_f(Q_i^s) = s_f(Q_i^e)$. Such a planar filling method will be an adaptation of the one developed in the lines wireframe case. More precisely, in order to match the curves ξ_i^s and ξ_i^e with tangent vectors $\mathbf{t}_i^s, \mathbf{t}_i^e$ at the points Q_i^s and Q_i^e , respectively, we construct a cubic Bézier curve with control points

$$\mathbf{b}_0 = Q_i^s, \quad \mathbf{b}_1 = Q_i^s + \sigma_1 \mathbf{t}_i^s, \quad \mathbf{b}_2 = Q_i^e - \sigma_2 \mathbf{t}_i^e, \quad \mathbf{b}_3 = Q_i^e,$$

with σ_1 and σ_2 being positive unknown parameters. This choice leads us to continuous tangent lines at Q_i^s and Q_i^e when filling ξ_i^s and ξ_i^e with (β_{ix}, β_{iy}) . In addition, curvature continuous condition at Q_i^s and Q_i^e determine the parameters σ_1 and σ_2 . It is worth noticing that in this case, as we are

matching plane curves, the continuity conditions of osculating plane and torsion are trivial, so that a cubic Bézier curve allows us to carry out the matching with continuous tangent lines and curvature at both ends points. It is easy to check that it is not possible to impose these conditions with a lower order Bézier curve.

- *Gradient lines wireframe:* In this case, for each $i = 1, \dots, p$, the couple of points $\{Q_i^s, Q_i^e\}$ can be arbitrarily chosen over ∂H^* . The curves $\{\xi_i^s, \xi_i^e\}$ are such that $\{s_f \xi_i^s, s_f \xi_i^e\}$ are the maximum gradient lines of s_f at $(Q_i^s, s_f(Q_i^s))$ and $(Q_i^e, s_f(Q_i^e))$ respectively. The β'_i 's are constructed as in the lines wireframe case, leading then to fillings with continuity of tangent lines, osculating planes, torsion and curvature at $(Q_i^s, s_f(Q_i^s))$ and $(Q_i^e, s_f(Q_i^e))$.

Remark 7. *It is to mention that contour and gradient lines criteria cannot be applied whenever the considered contour or gradient line of s_f at a point $Q \in \partial H^*$ lies over the boundary of H^* . Anyway it doesn't pose a problem since, apart from the fact that both drawbacks cannot happen at the same time at the same point, we can always move to another point Q over ∂H^* .*

It is important to point out that the choice of couples $\{Q_i^s, Q_i^e\}$ reveals to be crucial. In fact, choosing improper couple of points will give rise for sure to poor fitting patches. Regarding this issue, it is not possible to give a general criteria to choose $\{Q_i^s, Q_i^e\}$ leading to proper results in all cases. As expected -and checked in the experimental section-, doing a proper election strongly depends on the test function considered. Nevertheless, all experiments carried out show that there are two key aspects in order to obtain a proper wireframes family to fill the 'hole': (a) they must go through most part of it, i.e., relative big regions of the hole must not remain uncovered; and (b) they must faithfully gather the information of the shape of s_f near the inner boundary of $D - H^*$, and both aspects are absolutely conditioned by which the point $\{Q_i^s, Q_i^e\}$ be. Next we analyze how the choice of $\{Q_i^s, Q_i^e\}$ may affect (a) and (b) in each of the three families of wireframes considered.

The role of *lines wireframe* is to effectively cross the most part of the hole. As expected, numerical experiments show that lines wireframe criteria give very good fillings when s_f presents some kind of symmetry with respect to the hole. More precisely, in the examples carried out we have observed that the more the slopes of the tangent lines to the graphics of $s_f \xi_i^s$ and $s_f \xi_i^e$ at $t = 0$ are closer, the better the fillings β obtained through lines wireframes are. To this end, for each of the test functions we show a graphic in which, for 1920 points R uniformly distributed over ∂H^* , we associate a different level of blue according to the value of the directional derivative of s_f at R in the direction of the vector $\overrightarrow{R\mathcal{C}}$. More precisely, such directional derivatives are larger as color blue is deeper. Then, in

order to apply lines wireframe criteria, we have chosen the couples $\{Q_i^s, Q_i^e\}_{i=1}^p$ to have similar level of blue. This election will have a double beneficial effect: on the one hand, it will allow us to monitor the accomplishment of (b) above -to this end, we just have to choose couples covering a wide range of blue- and, on other hand, it will also allow us to *join* curves with similar slopes -to this end, we have to choose points $\{Q_i^s, Q_i^e\}$ having a similar level of blue-.

Regarding *contour lines wireframes*, we have considered that it might lead to good results as, somehow, they force the filling patch to have the z -component that it is expected to have. Of course, the effectiveness of the contour lines wireframe will depend on the shape of the function s_f and, more precisely, on the shape of its contour lines over $D - H^*$ and on the feasibility to fill them inside the hole H^* . In this family of wireframes, we can find that for a given starting point Q_i^s we may obtain multiple ending points. That's the reason why, in order to obtain proper ending points, we introduce contour lines map of function s_f over $D - H^*$. Observe that the contour lines map of the filling σ_{s_f} must reasonably *fill* the contour lines map of function s_f insofar as σ_{s_f} is expected to properly fill the hole inside s_f . Therefore, when multiple ending points are obtained, we are going to be able (in most cases) to obtain an appropriate ending paired point according to the map of contour lines of s_f over $D - H^*$. When working with contour lines wireframes (b) is somehow fulfilled as these lines gather the information of the paths over which s_f has a constant value and lead the way over which σ_{s_f} must keep these values. The unique issue then to monitor in this case is the accomplishment of (a), i.e., the global map of contour lines wireframes should somehow go through most part of the hole.

Finally, regarding *gradient lines wireframes*, there is no need to impose any particular initial conditions on starting and ending points. Gradient lines -which are called to complement contour lines ones insofar as they become a perpendicular system of curves- gather the information of maximum directional derivatives of s_f over ∂H^* and, therefore, they lead to high-quality starting and ending graphics over the holes, particularly when working with irregularly shaped functions, ensuring (b) above. In gradient lines criteria, it becomes particularly relevant the role of using Bézier techniques since having filling β_i strongly preserving the shape of the gradient lines considered over $D - H^*$ is absolutely crucial. As in the contour lines wireframes family, in this case we have just to monitor the accomplishment of (a).

It is to mention that (a) and (b) must be fulfilled by the complete set of wireframes, in such a way that one of the families considered may uncover one of both conditions whenever it is covered by another one (in the examples section we will check that for Franke's and Nielson's test functions, contour lines -or even gradient lines- wireframes lacks of (a), but the complete set of wireframes lead to good results since all of them cover (a) and (b)).

Next we will apply previous wireframe criteria to different test functions. We will analyze which of such criteria best suit to test functions considered depending on their particular shapes. A clear conclusion is that the best results are obtained when handling conjoint wireframes adapted to the particular shape of s_f .

In order to simplify the notation, all over the examples we will use the notation LW, CLW and GLW to refer to *lines wireframe*, *contour lines wireframe* and *gradient lines wireframe*, respectively.

Sinusoidal function:

We consider the function $f_1(x, y) = \sin(2\pi^2(x - 0.5)(y - 0.5))$ over $D - H_1$, where H_1 is the hole defined implicitly in (10), whose graphic is shown in Fig. 4.

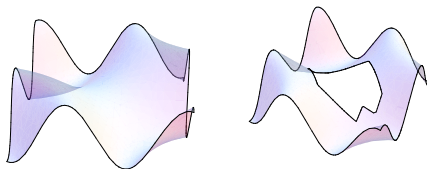


Figure 4: Function f_1 over D and over $D - H_1^*$.

The graphic of f_1 is symmetric with respect to the centroid of H_1^* , leading to a symmetric coloured plot of directional derivatives, as shown in Figure 5 left. As a consequence, any LW is expected to provide a proper filling curve β_i . For f_1 , we have considered the set \mathcal{Q} in (4) to be composed by $p = 8$ couples of points. In Figure 5, second, we plot the points \mathcal{Q} , the curves Ψ in (5) -the green ones inside the gray triangles of $(\mathcal{T}_{D-H_1^*}^{10})_6$ - and the fillings (β_{ix}, β_{iy}) for $i = 1, \dots, p$ -the green ones inside H_1^* -. In Figure 5, third, we show the graphic of s_{f_1} (the fitting one outside H_1^*) together with the ones of the filling wireframe β (7). In Fig. 5 right we show the joint graphics of s_{f_1}, β and of the filling $\sigma_{s_{f_1}}$ inside H_1^* .

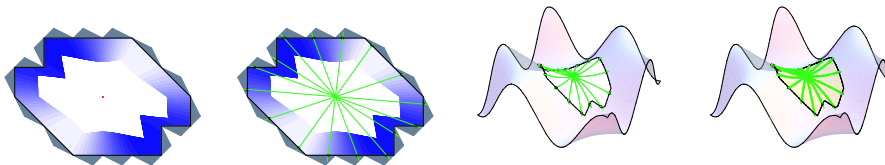


Figure 5: Plot of directional derivatives of s_{f_1} over ∂H_1^* (left) and lines wireframe for f_1 .

Despite the fact that LW works properly for sinusoidal function -due to the symmetry of its graphic-, we have also done tests with CLW and with GLW. In Figure 6 left we plot the contour lines map of s_{f_1} in $D - H_1^*$. When applying CLW to sinusoidal function we have found that for most starting points we have numerically obtained seven ending points -as expected from Figure 6 left-, but

just due to this figure we have been able to easily discard six of them. Results of CLW for f_1 are shown in Figure 6.

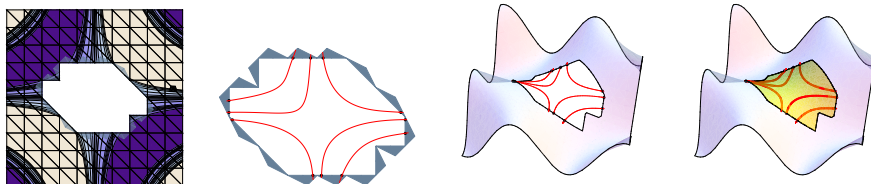


Figure 6: Contour lines of s_{f_1} in $D - H_1^*$ (left) and contour lines wireframe for f_1 .

Finally, in Figure 7 left we plot the gradient lines map of s_{f_1} at some points over ∂H_1^* and, as in the contour lines case, we choose the set \mathcal{Q} in order to (β_{ix}, β_{iy}) go through and cover H_1^* as much as possible. Results of GLW for f_1 are shown in Figure 7.

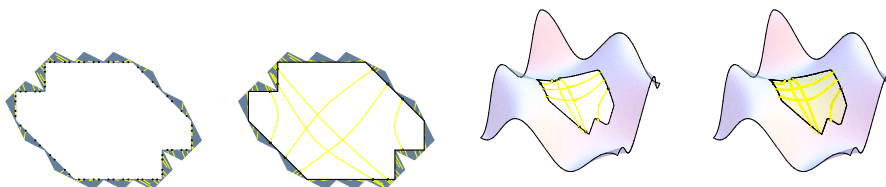


Figure 7: Gradient lines of s_{f_1} at points over ∂H_1^* (left) and gradient lines wireframe for f_1 .

In Tables 1 and 2 we show estimations of the relative errors committed inside the hole H^* when filling the test functions with the different wireframes proposed separately as well as with the joint set of wireframes. The relative error formula considered is

$$\frac{\sum_{i=1}^{2000} (f(a_i) - \sigma_{s_f}(a_i))^2}{\sum_{i=1}^{2000} f(a_i)^2},$$

where $\{a_1, \dots, a_{2000}\}$ are arbitrary points in H^* , f is the test function and σ_{s_f} is the filling function of f inside H^* . At the end of this section we include a brief analysis of the error estimations obtained.

In Figure 19 we show the joint wireframes considered for each of the test functions leading to errors in the last row of Tables 1 and 2.

Semisphere:

We consider the function

$$f_2(x, y) = \begin{cases} \sqrt{0.5^2 - (x - 0.5)^2 - (y - 0.5)^2} & \text{if } (x - 0.5)^2 - (y - 0.5)^2 \leq 0.5^2 \\ 0 & \text{otherwise} \end{cases}$$

over $D - H_1^*$, whose graphic is shown in Figure 8.

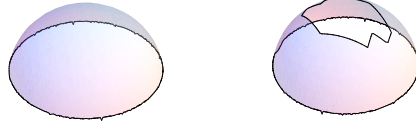


Figure 8: Function f_2 over D and over $D - H_1^*$.

In Figure 9 we show results for f_2 regarding LW. From left to right we show: the map of directional derivatives of s_{f_2} at points over ∂H_1^* together with the points \mathcal{Q} , the curves Ψ and the fillings (β_{ix}, β_{iy}) (left); the function s_{f_2} together with the fillings β (middle); the graphics of s_{f_2}, β and of the filling $\sigma_{s_{f_2}}$ inside H_1^* (right). Observe that in this case there exists also some kind of symmetry in the plot of directional derivatives and so it has been straightforward to choose points \mathcal{Q} . As for test function f_1 , we have also improved the filling of f_2 by using GLW. Results are shown in Figure 10 (from left to right: the gradient lines map of s_{f_2} at some points over ∂H_1^* together with the points \mathcal{Q} , the curves Ψ and the fillings (β_{ix}, β_{iy}) -left-; the graphics of s_{f_2} and β -middle-; the joint graphics of s_{f_2}, β and of the filling $\sigma_{s_{f_2}}$ inside H_1^* -right-). Observe that in Figure 10 left the different gradient lines do not pass exactly through the center $(0.5, 0.5)$ since the graph of s_{f_2} is not the semisphere, but an approximation. For test function f_2 we have not considered CLW criteria since the contour lines of s_{f_2} are almost circles centered at $(0.5, 0.5)$ and, therefore, they do not go significantly through H_1^* .

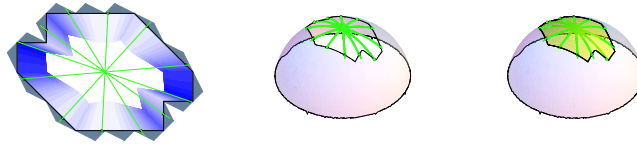


Figure 9: Lines wireframe for f_2 .



Figure 10: Gradient lines wireframe for f_2 .

Franke's function:

Next we consider Franke's function, defined by

$$f_3(x, y) = 0.75e^{-\frac{(9x-2)^2+(9y-2)^2}{4}} + 0.75e^{-\frac{(9x+1)^2}{10} - \frac{(9y+1)^2}{49}} + 0.5e^{-\frac{(9y-7)^2+(9x-3)^2}{4}} - 0.2e^{-(9y-4)^2-(9x-7)^2},$$

over $D - H_1^*$, whose graphic is shown in Figure 11.

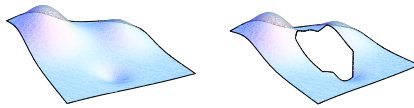


Figure 11: Function f_3 over D and over $D - H_1^*$.

In Figures 12, 13 and 14 we show results for f_3 by means of LW, CLW and GLW, respectively. Regarding LW, as in the previous cases, we have chosen the lines associated to closer directional derivatives of s_{f_3} over ∂H_1^* ; regarding CLW, according to Figure 13 left, we guess that contour lines of s_{f_3} may have a rather heterogeneous behavior inside H_1^* , not being for all starting points so easy to decide whether a candidate to ending point is suitable or not. So, we have just chosen a few of them which are closer to the boundary of H_1^* , which seem to present a predictable path. Finally, gradient lines have been chosen in order to go all through H_1^* and, somehow, report the information which is not covered by contour lines.

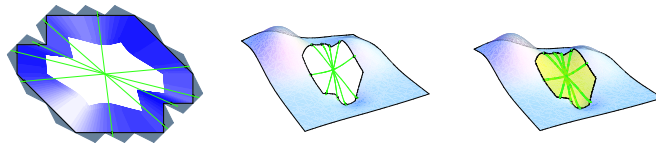


Figure 12: Lines wireframe for f_3 .

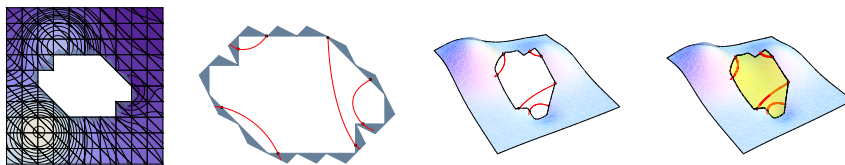


Figure 13: Contour lines wireframe for f_3 .

Nielson's function:

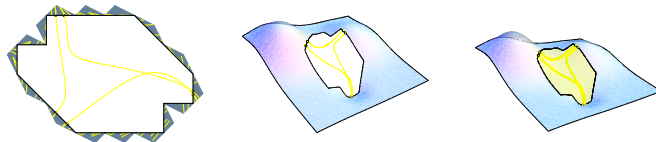


Figure 14: Gradient lines wireframe for f_3 .

Finally, we consider Nielson's function, defined by

$$f_4(x, y) = \frac{y}{2} \cos(4(x^2 + y - 1))^4,$$

over $D - H_2^*$, where H_2 (Figure 15 left) is defined implicitly by

$$\frac{(x - 0.6)^2}{0.19^2} + \frac{(y - 0.65)^2}{0.12^2} \leq 1.$$

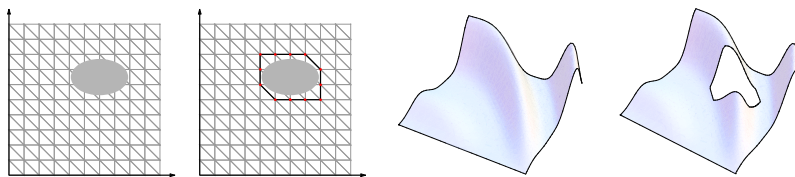


Figure 15: Hole H_2 , polygonal hole H_2^* and function f_4 over D and over $D - H_2^*$.

This is a more complicated example which requires a more detailed analysis and managing. The plot of directional derivatives of s_{f_4} over ∂H_2^* is shown in Figure 16. Although we could consider some lines to be filled with LW criteria, we observe that there are not too much options to consider couple of points, symmetric with respect to the centroid, with similar directional derivatives and covering a representative part of H_2^* . So, in this case, we have decided to start with CLW criteria. As for Franke's function, the plot of contour lines of s_{f_4} inside $D - H_2^*$ (Figure 17 left) is quite complex, not being easy to decide whether a candidate to ending point is suitable or not for all starting points. Therefore, according to this plot, we have chosen just contour lines that seem to have a predictable path. Results for f_4 by using CLW are shown in Figure 17. Of course, such contour lines are not enough to gather the particular shape of f_4 inside H_2^* , in such a way that the filling function when handling just CLW cannot be expected to be good, as shown in Figure 17 right. In order to overcome the lack of information about f_4 inside H_2^* when using just CLW, we are going to add some gradient lines in order to construct the filling σ_{f_4} . Such gradient lines will gather the information of maximum slope of s_{f_4} in perpendicular ways to

the contour lines and, therefore, the wireframe composed by all -contour and gradient- lines is expected to give a faithful filling function. Results are shown in Figure 18 right. Finally, in view of the filling function obtained with joint CLW and GLW (Figure 18 right), we have reinforced such a filling by means of a three lines wireframe strategically located in the ‘top’ of the graphic (Figure 19 right). Although visual appearance of such conjoint filling is the same than the one obtained just with CLW and GLW (Figure 18 right), in Table 2 we show that, indeed, the global filling is better when adding these lines to the wireframes CLW and GLW.

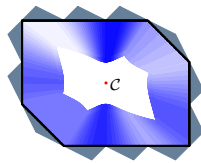


Figure 16: Plot of directional derivatives of s_{f_4} over ∂H_2^* .

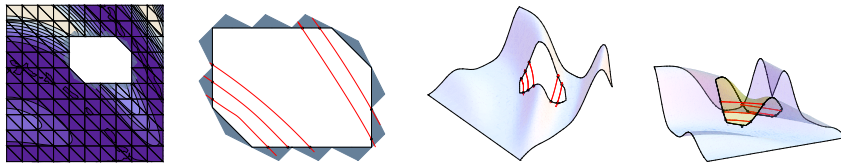


Figure 17: Contour lines wireframe for f_4 .

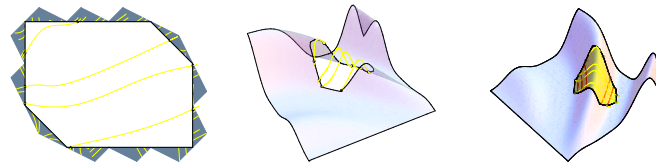


Figure 18: Gradient lines wireframe for f_4 .

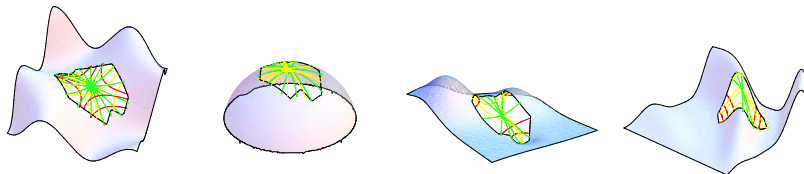


Figure 19: Joint wireframes of all test functions.

	f_1	f_2	f_3
<i>Lines wireframe</i>	$9.13 \cdot 10^{-5}$	$4.45 \cdot 10^{-4}$	$8.01 \cdot 10^{-4}$
<i>Contour lines wireframe</i>	$9.71 \cdot 10^{-5}$	—	$7.19 \cdot 10^{-3}$
<i>Gradient lines wireframe</i>	$7.15 \cdot 10^{-5}$	$4.32 \cdot 10^{-4}$	$4.31 \cdot 10^{-4}$
<i>Joint wireframes</i>	$1.03 \cdot 10^{-5}$	$5.71 \cdot 10^{-5}$	$8.41 \cdot 10^{-5}$

Table 1: Relative error estimations for test functions f_1, f_2 and f_3 .

	f_4
CLW and GLW	$6.17 \cdot 10^{-4}$
LW, CLW and GLW	$1.07 \cdot 10^{-4}$

Table 2: Relative error estimations for test function f_4 .

Regarding Tables 1 and 2 we can highlight the following facts: As i increases from 1 to 4, the shape of function f_i is more devious and thus, error estimations become slightly worse. Function f_1 is highly smooth over H_1^* and, therefore, LW, CLW and GLW lead to similar errors. In function f_2 we find that, due to its shape, LW and GLW are very close (see Figures 9 left and 10 left) and thus, error estimations are similar. The conjoint wireframe provides better results. Function f_3 presents the worst result for CLW, as expected insofar this wireframe on its own does not properly cover the hole. Error for GLW is better than the one for LW: somehow, GLW gathers and extends better the shape of s_{f_3} outside H_1^* . Finally, f_4 also presents better results when considering the conjoint frame. In fact, this is a common result: in all cases, the error estimations are better when considering joint families of wireframes.

In Table 3 we present a comparison of the orders of the best relative errors in this work (Tables 1 and 2) to the best ones provided in the following previous works covering the same topic of filling missing data: [5], where also a (weaker) *cartesian wireframe* of the filling surface is constructed, and [3], where the filling surface is constructed on a *shape-preserving* criteria which allows to estimate partial derivatives inside the hole. In [3] results of relative errors when filling just with a *minimal energy criteria* are also provided.

We can check in Table 3 that for all test functions we improve the results. Such an improvement is less significant for f_1 since it is a very smooth function, but we find it is relevant for the remaining test functions.

	Sinusoidal	Semisphere	Franke	Nielson
<i>This work</i>	$1 \cdot 10^{-5}$	10^{-5}	10^{-5}	10^{-4}
<i>Cartesian wireframe in [5]</i>	$8 \cdot 10^{-5}$	10^{-2}	10^{-3}	10^{-3}
<i>Shape-preserving criteria in [3]</i>	—	10^{-4}	10^{-4}	10^{-3}
<i>Minimal criteria in [3]</i>	—	10^{-3}	10^{-3}	10^{-1}

Table 3: Orders of the best relative errors when filling with different methods.

6. Conclusions

In this paper we have presented a method to fill the hole of a given surface (or dataset). The method consists of two stages:

- i*) To fit the given dataset by means of a quadratic \mathcal{C}^1 -surface s_f over a polygonal hole surrounding the original one;
- ii*) To define a filling patch σ_{s_f} interpolating some data of s_f over the boundary of the hole in order to the global function be quadratic and of class \mathcal{C}^1 .

The filling patch is obtained by faithfully extending the ‘shape’ of s_f inside the hole. To this end, we have decided to use Bézier curves, which provide a more suitable frame to work with geometric features and, therefore, are expected to lead to proper filling patches. Numerical and graphical results show that, indeed, the proposed method improves some of the previous filling methods results, specially when handling with devious shaped surfaces. All over the examples we check the relevant issue of adequately choosing the wireframe to be considered according to the particular shape of the function s_f to be filled.

Moreover, this paper naturally suggests to study the still unexplored field of filling patches by means of Bézier surfaces and, more particularly, of triangular patches, which has revealed to be a very natural way to represent splines defined over triangles. To explore the chances of using the geometric properties of the elevations of the control nets, as well as of the nets provided by the well known De Casteljaun algorithm when imposing geometric conditions to the filling patch, seems to be quite interesting.

Acknowledgements

Research partially supported by Ministerio de Ciencia, Innovación y Universidades (research project PGC2018-094898-B-I00) and by Consejería de Conocimiento, Investigación y Universidades of the Junta de Andalucía (research project FQM-191).

References

- [1] L.-C. Wang, Y.-C. Hung, Hole filling of triangular mesh segments using systematic grey prediction, *Computer-Aided Design* 44 (12) (2012) 1182–1189. doi:10.1016/j.cad.2012.07.007.
- [2] C. Wang, P. Hu, A hole-filling algorithm for triangular meshes in engineering, *International Journal for Computational Methods in Engineering Science and Mechanics* 14 (5) (2013) 465–471. doi:10.1080/15502287.2013.784385.
- [3] M. A. Fortes, P. González, A. Palomares, M. Pasadas, Filling holes with shape preserving conditions, *Math. and Comp. in Simul.* 118 (2015) 198–212. doi:10.1016/j.matcom.2014.12.008.
- [4] G. Farin, *Curves and Surfaces in CAGD. A Practical Guide*, 5th Edition, Morgan Kaufmann, 2002. doi:10.1016/B978-1-55860-737-8.X5000-5.
- [5] M. A. Fortes, P. González, A. Palomares, M. L. Rodríguez, Filling holes using a mesh of filled curves, *Math. and Comp. in Simulation* 164 (2019) 78–93.
- [6] M. Buhmann, *Radial basis functions: theory and implementations*, No. 12 in Cambridge Monographs on Applied and Computational Mathematics, Cambridge University Press, Cambridge, 2003.
- [7] G. Fasshauer, *Meshfree Approximation Methods with Matlab*, World Scientific Publishing Co. Pte. Ltd., Hackensack, NJ, 2007.
- [8] G. Taubin, An improved algorithm for algebraic curve and surface fitting, *Proceedings of the 4th International Conference on Computer Vision* (1993) 658–665. doi:10.1109/ICCV.1993.378149.
- [9] B. Jüttler, A. Felis, Least-squares fitting of algebraic spline surfaces, *Advances in Computational Mathematics* 17 (2002) 135–152. doi:10.1023/A:1015200504295.
- [10] J. H. Kappes, et al., A comparative study of modern inference techniques for discrete energy minimization problems, *Proceedings of the IEEE Conference on Computer Vision and Pattern Recognition* (2013) 1328–1335. doi:10.1109/CVPR.2013.175.
- [11] R. Szeliski, et al., A comparative study of energy minimization methods for markov random fields with smoothness-based priors, *Proceedings of the IEEE Transactions on Pattern Analysis and Machine Intelligence* 30 (6) (2008) 1068–1080. doi:10.1109/TPAMI.2007.70844.
- [12] A. V. Smurygin, I. V. Zhurbin, Biharmonic optimization of piecewise planar surfaces, *Optoelectronics, Instrumentation and Data Processing* 51 (2) (2015) 170–174. doi:10.3103/S8756699015020107.
- [13] C. Dyken, M. S. Floater, Transfinite mean value interpolation, *Computer Aided Geometric Design* 26 (2009) 117–134. doi:10.1016/j.cagd.2007.12.003.
- [14] V. Weiss, L. Andor, G. Renner, T. Várady, Advanced surface fitting techniques, *Computer Aided Geometric Design* 19 (2002) 19–42. doi:10.1016/S0167-8396(01)00086-3.
- [15] M. Botsch, L. Kobbelt, An intuitive framework for real-time freeform modeling, *ACM Transactions on Graphics* 23 (3) (2004) 630–634. doi:10.1145/1015706.1015772.
- [16] A. Jacobson, E. Tosun, O. Sorkine, D. Zorin, Mixed finite elements for variational surface modeling, *Computer Graphics Forum* 29 (5) (2010) 1565–1574. doi:10.1111/j.1467-8659.2010.01765.x.
- [17] O. V. Davydov, G. Nürnberger, F. Zefelder, Approximation order of bivariate spline interpolation for arbitrary smoothness, *J. Comput. Appl. Math.* 90 (2) (1998) 117–134. doi:10.1016/S0377-0427(98)00004-1.
- [18] M. Laghchim-Lahlou, P. Sablonnière, C^r -finite elements of Powell-Sabin type on the three direction mesh, *Adv. in Comput. Math.* 6 (1) (1996) 191–206. doi:10.1007/BF02127703.
- [19] M. J. D. Powell, M. A. Sabin, Piecewise quadratic approximations on triangles, *ACM Trans. on Math. Softw.* 3 (4) (1977) 316–325. doi:10.1145/355759.355761.

- [20] P. Sablonnière, Error bounds for Hermite interpolation by quadratic splines on an α -triangulation, *IMA J. of Numer. Anal.* 7 (4) (1987) 495–508. doi:10.1093/imanum/7.4.495.
- [21] D. Barrera, M. A. Fortes, P. González, M. Pasadas, Minimal energy surfaces on Powell-Sabin type triangulations, *Appl. Num. Math.* 58 (5) (2008) 635–645. doi:10.1016/j.apnum.2007.02.001.
- [22] D. Barrera, M. A. Fortes, P. González, M. Pasadas, Minimal energy C^r -surfaces on uniform Powell-Sabin type meshes: Estimation of the smoothing parameters, *Math. and Comp. in Simul.* 77 (2-3) (2008) 161–169. doi:10.1016/j.matcom.2007.08.020.